Environmental Science & Technology

pubs.acs.org/est

Article

# Determination of Microplastics' Vertical Concentration Transport (Rouse) Profiles in Flumes

Maximilian P. Born,* Catrina Brüll, Dirk Schaefer, Gudrun Hillebrand, and Holger Schüttrumpf

Cite This: *Environ. Sci. Technol.* 2023, 57, 5569−5579

Read Online

ACCESS | Metrics & More | Article Recommendations | Supporting Information

**ABSTRACT:** The transport behavior of microplastics (MPs) in the fluvial environment is scarcely researched. Besides settling velocities and critical shear stress for erosion, only a few investigations aim at MPs' vertical concentration profile and the underlying theory required. Therefore, this paper's experiments investigate vertical concentration profiles of approximately spherical MP particles ($d$ = 1−3 mm) with densities close to water (0.91−1.13 g/cm$^3$) in flow channels, coupling them with fundamental theory for the first time. The experiments were conducted in a tiling flume (slope of 0−2.4%) at 67 and 80 mm water depth, with a turbulent flow, velocities ranging from 0.4 to 1.8 m/s, and turbulence kinetic energy from 0.002 to 0.08 m$^2$/s$^2$. The measured profiles confirm the assumption that the concentration profile shapes of settling plastics are similar to those of sediments and running reversed for buoyant plastics. Furthermore, the hypothesis of the Rouse formula's applicability for floating and sinking plastics could be confirmed for approximately uniform flows. Future studies tying in with this research should increase particle properties and hydraulic parameter variation.

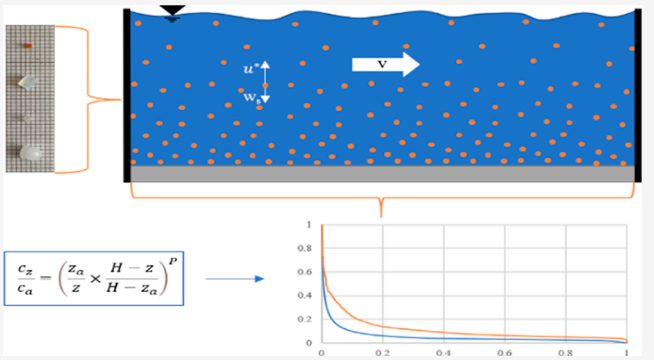


**KEYWORDS:** *microplastic, microplastic transport, Rouse profiles, microplastic concentration profiles, physical experiments, transport formula applicability*

## 1. INTRODUCTION

Plastics, produced on an industrial scale since the 1950s, are partly carelessly introduced into the environment, referred to as "littering".[2] Via various pathways, mainly wastewater, wind, and rain runoff, plastic enters rivers and finally deposits in sinks throughout the river's course or oceans.[3,4] Environmental factors acting on the plastics, such as UV radiation, degrade the plastic, inevitably fragmenting it due to mechanical forces.[5,6] According to the general scientific consensus, if these fragments are smaller than 5 mm, they are defined as microplastics (MPs).[7] However, this value represents only the upper margin. The classification ends at one micron.[8]

While research at the lower end of the size spectrum is still in its infancy, for MPs with a diameter of 330 $\mu$m and above, research questions have become more sophisticated, moving from oceans upstream toward the pollution's source.[9−12] However, this approach leads to several unresolved issues initially neglected in the ocean domain, e.g., the exact transport behavior. This matter becomes evident in numerical models simulating the transport of plastics in (flowing) water bodies.[13−16] However, derivations from related topics such as sediment transport may be too inaccurate.[17] Therefore, to express the behavior of plastics in water, fundamental data and general statements, in the form of equations, have to be developed through laboratory experiments, thus allowing numerical models to perform more precise calculations and increasing the process understanding. This demand for in-depth laboratory experiments is supported by, e.g., Jalón-Rojas et al. (2022),[18] who disproved the general assumption that forming a biofilm on a plastic particle will cause a faster descent.[19] Furthermore, in addition to natural influences on a particle, Xia et al. (2021)[20] revealed that the resuspension and vertical transport of sediment-burrowed particles in rivers are, besides hydraulic variations through varying discharges, dependent on human activity, e.g., ship traffic,[21] posing an additional influence to consider for transport models.

The vertical transport and concentration distribution of plastics in rivers bring relevance to sampling strategies besides their application in numerical simulations. The sedimentary equivalent was first published by Rouse in 1937, describing the sediment concentration in the water depth profile with 0.75−

Received: September 20, 2022
Revised: February 22, 2023
Accepted: March 8, 2023
Published: March 28, 2023





https://doi.org/10.1021/acs.est.2c06885
*Environ. Sci. Technol.* 2023, 57, 5569−5579

1.5 times accuracy of calculated versus measured values.[22] Several proposals for a modified Rouse equation aiming for an improved concentration distribution approximation were published throughout the years, as Cheng et al. (2013)[23] summarized. However, Rouse's research and its modifications referred to sediments with a density of about 2.65 g/cm$^3$. The first theoretical attempts to apply Rouse's equation to MPs were conducted by Cowger et al. (2021),[24] although Muste et al.[25] investigated the concentration distribution of MP particles in an experimental study already in 2009. However, whether Rouse's formula, which is still frequently used today, can be transferred onto plastics with strongly deviating densities and partly buoyant properties has not yet been experimentally investigated and represents the core question of this paper.

## 2. THEORY

Particle transport in rivers occurs primarily in longitudinal and vertical directions, although laterally directed transport also exists but lies beyond this paper's scope. In a fully stagnant water column, the vertical particle transport direction depends only on its density ($\rho_s$); at densities above water's ($\rho_w$), the particle sinks and vice versa for lower densities. The resulting settling (↓) or rising (↑) velocity ($w_s$) is strongly influenced by the shape of the particle, described by a drag coefficient, defined here as the shape coefficient ($C_D$), which includes surface roughness as well.[26,27] In principle, the velocity's attenuation increases proportionally with expanding working surface area (often, the surface-to-volume ratio is also used).[28−30] However, the classical equation for terminal velocity assumes particles to be spherical, and their diameter ($d_s$) is applied (eq 1).

$$w_s = \sqrt{\frac{4}{3}\frac{g \cdot d_s}{C_D}\left(\frac{\rho_s - \rho_w}{\rho_w}\right)} \tag{1}$$

Transport in the longitudinal direction is caused by longitudinally directed flow in a water body. In a purely longitudinal and laminar flow, particles with a density below 1 g/cm$^3$ would be transported at the water surface and the bed for particles above 1 g/cm$^3$. However, most solids are transported between these boundaries since turbulent flow is predominant in rivers.[31] The mode of transport is divided into bed transport, suspended transport, and wash load. To estimate the prevalent transport mode within given boundaries, the Rouse number ($P$) (eq 3), developed by Hunter Rouse, can be utilized (Table 1). This equation relates the terminal settling velocity (positive in the sinking direction) to the opposing influences, the product of the von Karman constant ($\kappa$ = 0.41), and the (bed) shear stress velocity ($u^*$).[32] For uniform flow conditions, the (bed) shear stress velocity can be derived from eq 2, employing the hydraulic radius ($R_h$) and the (surface) slope ($S$). The factor ($\beta$) correcting for eddy diffusion derived from eddy viscosity, although usually set to 1, can vary throughout the water column.[33,34]

$$u^* = \sqrt{\frac{\tau_0}{\rho_w}} = \sqrt{\frac{\rho_w \cdot g \cdot R_h \cdot S}{\rho_w}} \approx \sqrt{g \cdot R_h \cdot S} \tag{2}$$

$$P = \frac{w_s}{\beta \cdot \kappa \cdot u^*} \tag{3}$$

Moreover, the Rouse eq 4, derived from the advection-diffusion equation, assuming a uniform, steady, and not upward-facing flow, determines the local concentration of a substance ($c_z$) as a function of a known Rouse number ($P$) at depth ($z$) for a known total water depth ($H_T$).[32] A reference concentration ($c_a$) at a known depth (usually $\Delta z_a = k_s/32$; with $k_s$ [mm] as bed roughness defined as Nikuradse's equivalent sand roughness) is required further.[35] If only a normalized concentration profile is desired, $c_a$ is not a premise since $c_z/c_a$ = 1 for $z = z_a$. Furthermore, Rouse developed Rouse profiles from the equation, plotting normalized particle concentration versus normalized water depth.

$$\frac{c_z}{c_a} = \left(\frac{z_a}{z} \cdot \frac{H_T - z}{H_T - z_a}\right)^P \tag{4}$$

However, besides their theoretically universal applicability, the developed equations were primarily designed to describe the behavior of sediments with densities of around 2.65 g/cm$^3$. Whether this theoretical applicability is also valid for particles with densities below 1 g/cm$^3$ has been insufficiently considered and only addressed theoretically by Cowger et al. (2021).[24] In the corresponding study, the authors propose extended Rouse number ranges for particles with negative settling velocity based on the gradations for sinking particles with reversed signs (Table 1).

It remains unclear whether this assumption is applicable as no published laboratory studies dealing with negative Rouse numbers exist.

However, whether a negative Rouse number can be readily adopted is questionable because the influence of near-bed shear stress at the water surface, especially for greater water depths, approaches zero.[36] Furthermore, the Rouse number reflects the relationship between the settling velocity and the influences counteracting it. Since turbulences (i.e., velocity fluctuations) are upward- and downward-facing, the turbulent diffusion counteracts the settling velocities independent of the sign of the settling velocity. However, the influence of shear stress would only be possible if the assumption holds that Reynolds' shear stress ($\tau_{turb}$) is equal to the near-bed shear stress ($\tau_0$), i.e., $\tau_{turb} \approx \tau_0$ applies.[25,37] This would also imply that increased turbulence and ergo higher velocities (at constant geometry and viscosity), expressed in terms of Reynolds number, result in increased transport of buoyant particles into the water column. Other simplifying assumptions, such as constant Rouse number throughout the water column, must be re-examined for applicability in the negative Rouse number domain.[33,34]

Further deviations might occur, transferring the theoretical approach of suspended sediment particles to plastics. While the

**Table 1. Negative Rouse Number Ranges by Rouse (1937)[22] and as Proposed by Cowger et al. (2021)[24] and Their Respective Corresponding Mode of Transport**

| Rouse number range by H. Rouse (1937)[22] | mode of transport |
|---|---|
| $7.5 < P$ | no transport |
| $2.5 < P < 7.5$ | bed load transport |
| $0.8 < P < 2.5$ | suspended transport |
| $0 < P < 0.8$ | wash load |
| **Rouse number range by Cowger et al. (2021)[24]** | **mode of transport** |
| $-0.8 < P < 0.8$ | wash load |
| $-2.5 < P < -0.8$ | rising suspended transport |
| $P < -2.5$ | surface transport |



https://doi.org/10.1021/acs.est.2c06885
Environ. Sci. Technol. 2023, 57, 5569−5579

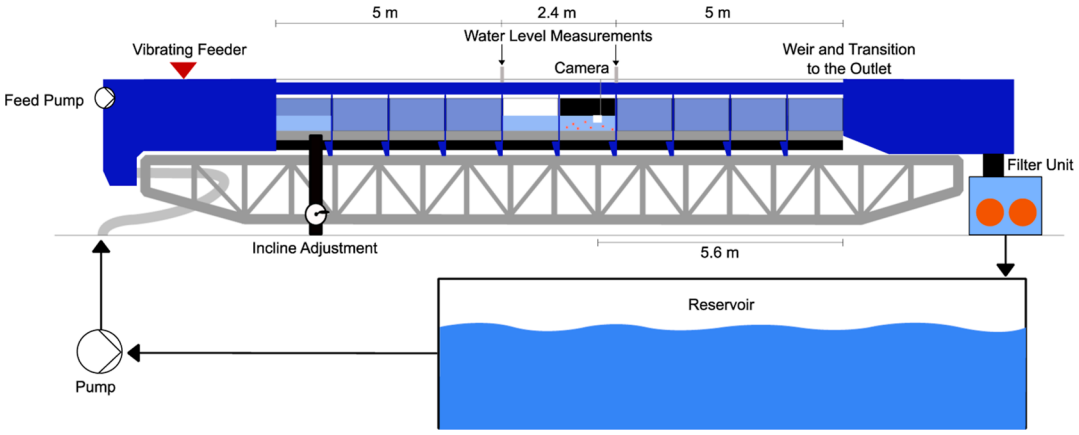


**Figure 1.** Small tilting flume of the IWW. $L$ | $W$ | $H$: 17 m (12.4 m experimental environment) | 0.3 m | 0.32 m. The order of arrangement of the other components—filter unit, reservoir, and pump—is shown in the process diagram. Oriented at the studies from Freyer (2023).[1]

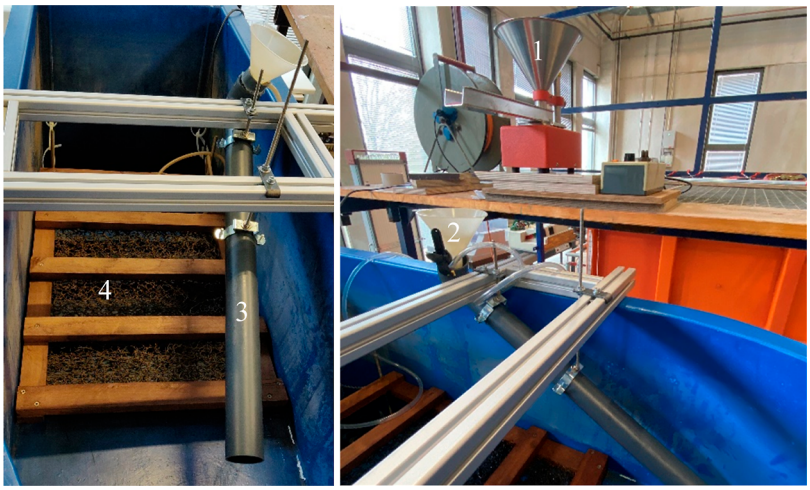


**Figure 2.** Vibration feeder (1) and anti-air-adherence setup for the particle dosing [funnel with water supply (2) and pipe with 35° inclination (3)]. Furthermore, the flow equilization is visible (4).

former is not perfectly spherical, possibly deviating significantly, plastic shapes scatter almost unlimited.[6] In addition to widely varying shapes, certain plastics can change shape during transport, as in the case of films [Kuizenga et al. (2021).[30] Since the Rouse number requires the terminal settling velocity, requiring the shape coefficient ($C_D$), an exclusively theoretical approximation of the coefficient will likely result in a deviation from the actual settling velocity. The much-cited formulas of Waldschläger and Schüttrumpf (2019),[28] representing a significantly improved approximation compared to previous approaches, show an average relative measurement error ($E$) of 27 and 21%, respectively, despite a coefficient of determination ($R^2$) of 0.83 (sinking) and 0.97 (rising), not including foils. However, a recent study by Kuizenga et al. (2021)[30] found a first promising approach for foils and films. Van Melkebeke et al. (2020)[38] summarized all existing models [up to 2020, thus leaving out Karkanorachaki et al. (2021)[39] and Jalón-Rojas et al. (2022)[18] for shape coefficient calculation and found that the average error was lowest at 13% and up to 48%. The approximations represent a significant improvement over sediment-based approximations for numerical simulations, modeling the behavior of plastics. However, they cannot replace a settling velocity determination in laboratory tests if reliable and precise statements, such as those concerning the negative Rouse number range, are desired. Computationally approximated shape coefficient models [like Cowger et al. (2021)[24] only allow a statement about the range of values included in the approximation, not beyond.

The theory section reveals that the knowledge on Rouse profiles for sediment-deviating shapes and densities is insufficient for a reliable theoretical discussion, while crucial assumptions for its applicability, such as $\tau_{turb} \approx \tau_0$, were concluded from the presented theory. The need for in-depth experimental research on this topic can therefore be concluded. Thus, the upcoming section will describe the methodological approach to measuring the concentration profiles of various plastic particle types in a turbulent flow.

## 3. METHODS

Particle transport experiments in a flume (Figure 1) were carried out by adding different MP types into the water at the inlet and observing their vertical transport behavior mid-flume. The experiments were conducted to determine the concentration profiles of MPs and therefore recorded with a camera and evaluated via various software. In addition, several monitoring tools for the hydraulic settings of the flume were used.



https://doi.org/10.1021/acs.est.2c06885
Environ. Sci. Technol. 2023, 57, 5569−5579

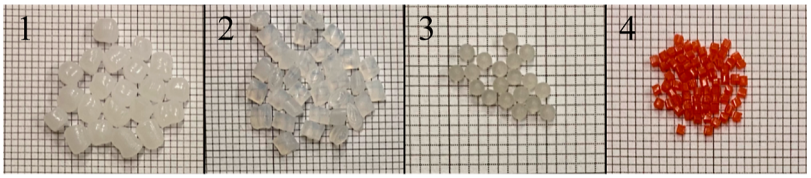


**Figure 3.** (1) White PE-HD granules diameter approx. 3 mm, density approx. 0.94 g/cm$^3$. (2) White PA6 plate cylinders 3 | 1.5 mm, density, according to the manufacturer, 1.13 g/cm$^3$ (3) Milky-white PP spheres 1.5 mm, density approx. 0.91 g/cm$^3$. (4) Red PA6 cubes 1 mm, density approx. 1.11 g/cm$^3$. All particles of one plastic particle type had a similar or the same shape. Densities were determined according to DIN EN ISO 1183-1:2019-09.

**Table 2. Hydraulic Parameters and Flume Configurations for Every Run**[a]

| settings for PE-HD and PP* (↑) | | | | settings for both PA6 particle types (↓) | | | |
|---|---|---|---|---|---|---|---|
| water level (m) | flow velocity (m/s) | discharge (m$^3$/s) | flume-slope (%) | water level (m) | flow velocity (m/s) | discharge (m$^3$/s) | flume-slope (%) |
| | | | | *0.08* | *0.4* | *0.0096* | *0* |
| | | | | 0.08 | 0.5 | 0.012 | 0.04 |
| | | | | 0.08 | 0.6 | 0.0144 | 0.17 |
| | | | | 0.08 | 0.7 | 0.0168 | 0.24 |
| | | | | 0.08 | 0.8 | 0.0192 | 0.31 |
| *0.067* | *0.9* | *0.0181* | *0.44* | <u>0.08</u> | <u>0.9</u> | <u>0.0216</u> | <u>0.39</u> |
| 0.067 | 1 | 0.0201 | 0.54 | 0.08 | 1 | 0.024 | 0.48 |
| 0.067 | 1.1 | 0.0221 | 0.61 | 0.08 | 1.1 | 0.0264 | 0.6 |
| 0.067* | 1.2* | 0.0241* | 0.69* | 0.08 | 1.2 | 0.0288 | 0.71 |
| 0.067 | 1.3 | 0.0261 | 0.81 | 0.08 | 1.3 | 0.0312 | 0.84 |
| <u>0.067*</u> | <u>1.4*</u> | <u>0.0281*</u> | <u>1.02*</u> | 0.08 | 1.4 | 0.0336 | 0.98 |
| 0.067 | 1.5 | 0.0302 | 1.23 | **0.08** | **1.5** | **0.036** | **1.19** |
| 0.067* | 1.6* | 0.0322* | 1.49* | | | | |
| 0.067 | 1.7 | 0.0342 | 1.75 | | | | |
| **0.067*** | **1.8*** | **0.0361*** | **2.42*** | | | | |

[a]The weir was used for the runs with 0.4 and 0.5 m/s flow velocity to ensure 0.08 m water depth. The velocities referred to as lowest (italics), medium (underlined), and highest (bold) tested velocities for the respective water depth are highlighted.

**3.1. Model Setup.** The experiments were conducted in the Institute of Hydraulic Engineering and Water Resources Management Laboratory at RWTH Aachen University (IWW). A tilting flume was used for the experiments (Figure 1).

The flume's discharge is freely adjustable, up to a maximum of 0.0361 m$^3$/s, measured inductively with an accuracy of ±0.5%, and is equalized directly above the inlet via a woven mat (Figure 2). Furthermore, the flume is continuously tiltable from −0.5 to 2.5%. The desired values were initially surveyed and controlled for every setting with a precision of ±1 mm/50 m. The resulting maximum average flow velocity is 1.81 m/s. Furthermore, the water depth can be controlled independently of slope and discharged via a moveable weir at the flume's end. Two ultrasonic leveling sensors framing the experimental section can be used for water-level measurements with an accuracy of ±1%.

The flow and water depth measurements allow precise adjustments of the flow velocity and, thus, the repeatability of the experiments. An intermediate reservoir, which filtered all particles through a sieve (mesh size 0.3 mm), was constructed to avoid particle contamination from previous tests and the pollution of the water circuit's main reservoir. Furthermore, the main reservoir ($V \approx 100$ m$^3$) was regularly cleaned. The water temperature was around 20 °C throughout the experiments.

**3.2. Particle Injection.** A constant particle input had to be ensured for the experiments. This mainly roots out of two reasons. First, too-elevated concentrations cause particles to tumble over each other, which thus experience an increased and unequal angle of attack, reducing the comparability with other runs. Second, the experiments' reproducibility could thus be ensured. A vibrating feeder (*FRITSCH Laborrette 24*) was used for particle metering, allowing a constant, precisely adjustable feed of plastic particles (Figure 2).

One of the essential parameters in transport tests of plastic particles is the exclusion of air on the particle surface since it massively changes the density and, thus, the transport properties. Preliminary tests revealed that different approaches were necessary for particles with densities above and below water. The surface tension combined with the resulting buoyancy force of buoyant particles required increased outlet height difference to the water surface so these could penetrate it in the same manner as sinking particles. These tests also revealed that adhering air diffuses into the water after a certain period. However, the required residence time was above the transport duration of the particles in the flume, thus requiring an anti-air-adherence setup.

For sinking plastics, particles were metered into a pipe with an inclination of 35° via a funnel as the inlet. Parallel to the flume, this pipe was fed with water at a flow rate of 50 mL/s (an extra pump drew from the flume, not changing $Q_{tot}$) (Figure 2). The inclination and the water flow rate led to air-free feed, exclusively in this ratio. The water surface penetrating pipe fed the particles in a calm part to prevent air from adhering to the particles due to a turbulent surface. The particle velocity achieved by slope and flow within the pipe was sufficient for the particles to penetrate the water surface without drawing in air.



https://doi.org/10.1021/acs.est.2c06885
Environ. Sci. Technol. 2023, 57, 5569−5579

The same slope and flow rate were chosen for particles with densities below 1 g/cm$^3$. However, the particles had to penetrate the water surface; otherwise, they remained at the water surface, even at the intense inlet turbulences caused by the discharge entering the flume from the pump. This would have resulted in a different particle transport starting location in the water column compared to sinking particles. Thus, the outlet was positioned 2.5 cm above the water surface to compensate for this deviation, guaranteeing a similar transport starting location. These settings resulted in air(-bubble)-free particles, with only a few exceptions, monitored with the slow motion recording of the camera.

**3.3. Material.** The experiments were carried out with four different particle types, two with a density above and two below 1 g/cm$^3$ (Figure 3). The particles were intentionally oriented as close as possible to the density of water since the transport throughout the water column is critically dependent on the density difference between water and the transported particle.

**3.4. Experimental Program and Settings.** After the hydraulic and flume parameters were set as desired, the main pump was switched on for the experiment (Table 2), and the particle feed pump and the metering unit started. Next, a start-up period was defined to achieve a constant concentration distribution (determined by a scale; ±0.01 g, measuring the particle flow for 30 s), whereupon the recording was started. Over the 30 s recording time, approximately 2000 particles (depending on the plastic type) were metered into the channel and recorded.

The flume's center (camera position 2 in Figure 1) was selected for the experiment recording, allowing the best possible reduction of inlet and outlet effects, as flow equalization and the exclusion of water level changes caused by the weir met at this position. A water depth of 8 cm was selected for the tests, keeping the water level constant across almost all flow velocities by adjusting the discharge, slope, and weir. However, for plastic types requiring the flume's maximum velocity (1.81 m/s), the water level had to be lowered to 6.7 cm through a 2.4% slope at 36.1 L/s discharge. The exact values can be found in Table 2 and additional values in the Supporting Information (Tables S1−S3).

The minimum experimental flow velocity for sinking plastics (0.4 m/s) was oriented at the transition of bed load to suspended particle transport. A fixed value had to be chosen despite the stochastic nature of the transition from bed load to suspended transport of particles. The transition of bed load to suspended transport was defined by the first particle moving more than 10 times its diameter in the water column. The velocity causing more than 1% of the particles to reach the water surface was set as the maximum velocity and upper boundary (1.5 m/s). This approach was based on the fact that from then on, no statement about the behavior of the particles at a potentially increased water depth of more than 8 cm is possible. The boundary conditions were reversed for plastics with a density below water, ranging from 0.9 to 1.8 m/s experimental velocities.

Since vertical velocities of particles are a decisive factor for their transport in water, rising and settling tests were carried out for all particle types with a sample size of 15 particles, inspired by the procedure of Waldschläger and Schüttrumpf (2019)[28] and Waldschläger et al. (2020),[29] respectively. First, a measurement section length was defined, and its ends were marked. Then, identical cameras were aligned perpendicularly on each marking, which could be started synchronously. Furthermore, a high recording frequency of 60 Hz guaranteed that sinking and rising velocities could be determined with an accuracy of ±0.4%.

**3.5. Recording.** The camera's (GoPro Hero 8) settings used to record the experiments were a recording frequency of 120 Hz, a shutter speed of 1/480 s$^{-1}$, and a resolution of 1080p. These requirements result from the small size of the particles combined with high velocities of up to 1.81 m/s. A deviation from these values, especially the shutter speed, leads to a distortion in the recording and a significantly deteriorated evaluation. The camera also featured image stabilization and a linear shooting mode compensating for lens curvature and was positioned at a 33 cm distance from the flume's center.

In order to ensure sufficiently bright images at low exposure times, the camera setup mounted on the flume was equipped with high-performance LEDs. In addition, the channel bottom and the wall opposite the camera were covered with matt-black adhesive foil to exclude the resulting particles' and turbulences' shadows. The foil was also necessary to achieve sufficient contrast for the images. Furthermore, the recording section was darkened entirely to exclude ambient reflections.

The recording time resulted from limitations of the intermediate reservoir's filter, which accumulates the particles with increasing experimental duration, reducing the discharge. High flow rates resulted in an overflow of the intermediate reservoir within 1 min. Furthermore, 7200 images were recorded within 30 s, almost wholly occupying the PC's RAM (64 GB) during the evaluation.

In addition, 3D-velocity measurements with a sideward facing acoustic-doppler-velocimeter (ADV)—*VECTRINO SIDE CABLE PROBE 10 MHz, NORTEK AS*—were conducted throughout the water column with 5 mm steps for every experimental setting to evaluate the turbulence kinetic energy (TKE) of the flow. The TKE is a vital parameter since it quantifies local turbulences, the main driver for particle entrainment from the water surface and particle transport throughout the water column. However, the ADV cannot measure velocities close to the surface due to air entrainment and its size. The measurements thus end at around 2−3 cm below the surface. Therefore, the TKE above the working range might be approximated via extrapolation of the measured values.

**3.6. Data Evaluation.** Four programs were used to evaluate the recordings. First, the videos were exported into individual frames with the program *ShotCut*.[40] Afterward, the images were converted to grayscale (32 bit) for increased contrast, and, in some cases, the saturation was adjusted in the program *Fiji/ImageJ*.[41] Next, the images could be further analyzed with the *Fiji/ImageJ* add-in *TrackMate*.[42,43] The particle tracking program was used to detect the plastic particles, and the results were manually controlled. The position of each particle in a frame could be exported as X/Y pixel values. A *MatLab*[44] application developed by the research team was then used to create a concentration profile.

The bottom ($Y_{min}$) and water surface ($Y_{max}$) can be specified as pixel values. The program then divides the water column with horizontally defined lines into the desired number of vertical sections of equal size, 25, for the experiments presented in this paper. Each section is assigned a $Y_{i;min}$ and $Y_{i;max}$ value. The raw data from *TrackMate* are then imported, corrected with factors for the refraction of water and glass, and the resulting *Y*-values of the particles are assigned to the



https://doi.org/10.1021/acs.est.2c06885
Environ. Sci. Technol. 2023, 57, 5569−5579

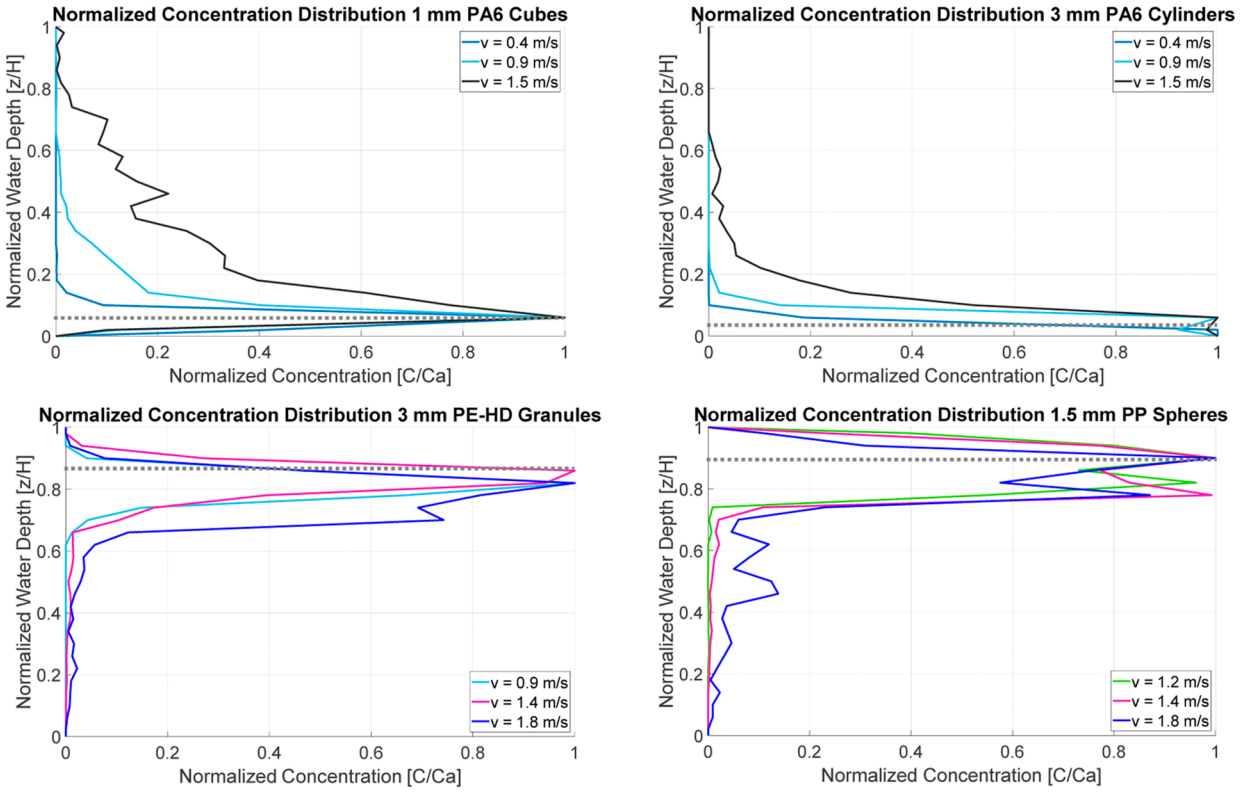


**Figure 4.** Rouse profiles of all plastics investigated. The velocities displayed are the flumes lowest, intermediate, and highest velocity configurations. All other plots can be found in the Supporting Information (Figure S5) but were left out here for a more transparent overview. The gray dotted lines represent the factual water surface and bed (Section 3.6). Theoretical calculations for sediments with the experimental settings yielded Rouse numbers between 18.2 and 5.4, thus either no or only bed load transport, deviating strongly from the plastics.

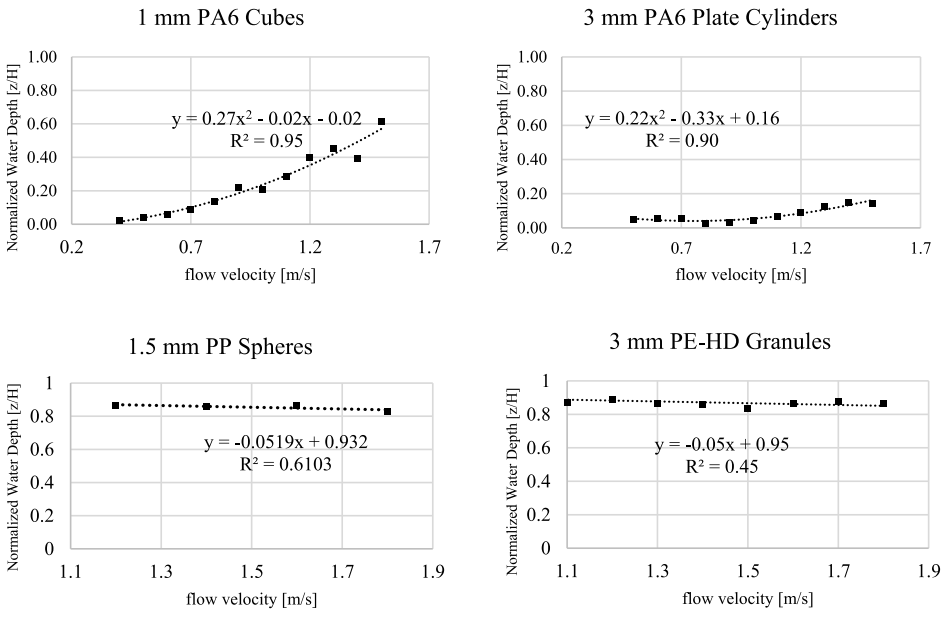


**Figure 5.** Graph courses of the normalized water depth at which the 10% normalized particle concentration was achieved ($Y$-axis) over the corresponding velocities (m/s | $X$-axis) for all velocity settings and particle types investigated.

respective sections. Thus, a particle count ($P_i$) is available for each section. To generate a concentration comparable with the Rouse equation, $P_i$ is divided by a reference particle count ($P_{ref}$), and thus, a normalized concentration value ($C_{P,i}$) at water depth $Y_i$ ($= (Y_{i;max} + Y_{i;min}) \times 0.5$) is generated. A section close to the surface was defined as the $P_{ref}$-section for particles with densities above and a near-bed section for particles below water. However, the particle sizes themselves, combined with bottom unevenness in the flume, and turbulences slightly altering the water surface position over time, left a range of pixel values considerable as the bed and water surface. However, to evaluate all particles, the boundary pixel values



https://doi.org/10.1021/acs.est.2c06885
Environ. Sci. Technol. 2023, 57, 5569−5579

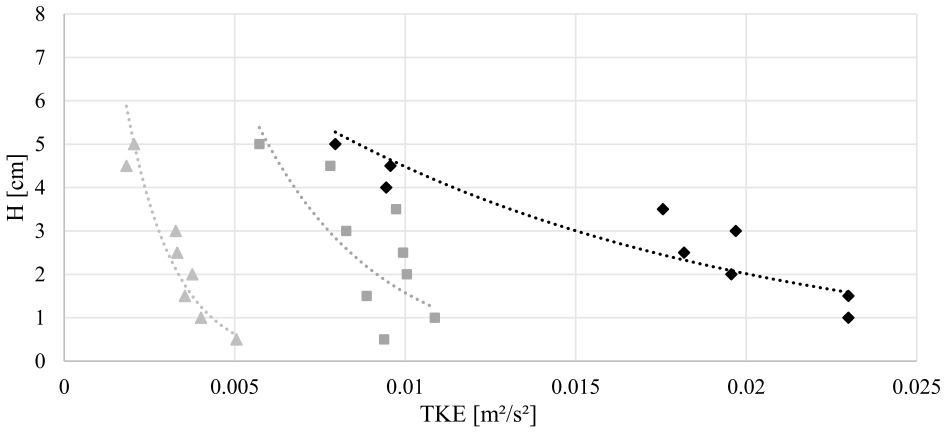


**Figure 6.** TKE distribution for a total water depth of 8 cm for 0.4 m/s (light gray, triangles), 0.9 m/s (dark gray, squares), and 1.5 m/s (black, diamonds) mean flow velocities. The trend lines were calculated with an exponential fit ($e^x$) for improved clarity of data point coherence.

must lie outside the pixel values of all detected particles, resulting in sections partly outside the water column. Thus, the reference sections had to be adjusted to the factual surface and bed.

The normalization of water depth ($H_{Y;i}$) at point $Y_i$ is conducted using $H_{Y;i} = Y_i/(Y_{i;max} - Y_{i;min})$. Subsequently, the generated points are plotted (linearly interpolated) with $H_Y$ on the $Y$-axis (independent of the particle density) and $C_P$ on the $X$-axis. Thus, $H_y = 0$ describes the bed, and $H_y = 1$ describes the surface.

## 4. RESULTS

Approximately 200,000 MP particles were used for the experiments, and their positions were evaluated. The normalized concentration distributions throughout the water column are presented as graphs and not numerically in this section for an improved overview (Figure 4). In addition, to describe the increased amount of particles transported in the suspension with increasing velocities and turbulences, the water depths at which the particle concentration reaches 10% (for the first time) are plotted as a function of velocity (Figure 5). Detailed data tables on flume settings, flow characteristics, concentration plots for all velocities, comparisons of measured versus calculated concentrations, and TKE throughout the water column are attached in the Supporting Information.

For a more transparent overview, the graphs in Figure 4 represent the concentration profiles of the plastic particles at the lowest (0.4 m/s ↓ | 0.9 m/s ↑/1.2 m/s ↑), medium (0.9 m/s ↓ | 1.4 m/s ↑), and highest (1.5 m/s ↓ | 1.8 m/s ↑) averaged flow velocities used for the respective plastic-type, with the normalized concentration on the $X$-axis and the normalized water depth on the $Y$-axis. Thus, $Y = 1$ is the water surface, while $Y = 0$ is the flume's bed. For sinking particles, the concentrations are highest near the bed. Thus, the normalized concentration is around 0 at the surface and almost 1 at the bed for every graph. For rising particles, the concentration is highest near the surface. All graphs in Figure 4 contain a break-off at approximately 0.1 or 0.9 normalized water depth at the actual bed and water surface (as described in Section 3.6). The factual water surface and bed are included in the graphs of Figure 4 as gray dotted lines. For the evaluation, the data were adjusted for the offset. Further concentration profiles can be examined in the Supporting Information (Figure S5).

The graphs' course in Figure 4 is comparable to a classical sediment transport profile for the plastic particles with a density above water's. It is evident that at higher velocities, ergo increased near-bottom shear stress and turbulences, the mode of transport moves from almost pure bed load (0.4 m/s-graph) toward suspended transport (1.5 m/s-graph). Correspondingly, the particle distribution shifts toward the surface with increasing velocities in an exponential manner (2nd degree), observable in the top left plot of Figure 5. Additional influences on the concentration profiles become evident by comparing the deviating particle sizes at the same density of PA6. Although the concentration in the water phase (Figure 4) also rises with increasing flow velocities for the 3 mm PA6 particles, it is significantly lower than that for the 1 mm PA6 particles. Even at 1.5 m/s, the 3 mm PA6 particles distribute almost closer to the bed (gray dotted line) than the 1 mm PA6 cubes at 0.9 m/s.

This behavior is again evident when considering the water depth at which 10% of the maximum concentration is present, which generally shifts toward the surface with increasing velocities for particles with a density above 1 g/cm$^3$ (Figure 5). Figure 5 contains the trend lines of the spots for the water depth at 10% $C_a$ for each velocity, further indicating the increasing dispersion of particles transported in the suspension. The described shift is exponential for the 1 mm PA6 cubes up to 0.6 but almost linear for the 3 mm PA6 particles at a maximum of 0.15 [still having a better coefficient of determination ($R^2$) utilizing a quadratic approximation].

The assumption of similar behavior for particles with a density below 1 g/cm$^3$ is quickly disproved by comparing the respective graphs, presented left and right at the bottom in Figures 4 and 5. Although the polyethylene high density (PE-HD) particles have twice the diameter of the polypropylene (PP) particles, the concentration graph does not change comparably to the two PA6 particle types. Instead, despite a high number of particles, reruns, and thus statistically meaningful results, the change in the course is more variable, and the graphs partially intersect. Only at the highest velocities (Figure 4 | 1.8 m/s | blue), a more pronounced difference in the concentration curves does occur. The difference in density between the particles is about 4%. Furthermore, their water depth shift in Figure 5 can be described best through a linear approximation, although the data for PP particles are most likely too scarce for a meaningful statement.

The displayed shift in Figure 5 presents the direct dependency of the particle distribution throughout the water column on the (turbulent) energy present in the flow since



https://doi.org/10.1021/acs.est.2c06885
Environ. Sci. Technol. 2023, 57, 5569−5579

increased velocities at a constant water depth result in increased total energy of the flow. However, the transport perpendicular to the main flow direction is only possible via upward- and downward-facing turbulences. Since turbulences are a deviation from the time-averaged mean flow, they can be described via the TKE. The TKE sums up the mean variances from the time-averaged flow conditions in $X$, $Y$, and $Z$ orientation, incorporating them into the kinetic energy calculation while excluding the mass [thus, the TKE is a turbulent kinetic energy density ($J/kg = m^2/s^2$)]. TKE is highest near the bed, where flow velocity gradients are large. Figure 6 exemplarily shows the TKE distribution throughout the water column at 0.4, 0.9, and 1.5 m/s. The increased TKE is manifested in the plots of Figures 4 and 5, which present a concentration shift for increasing mean velocities. Additional TKE plots for all velocities can be found in the Supporting Information (Figures S6 and S7).

In addition to the particle dimensions, the particle shape is also a relevant factor for MP transport.[28,29] Therefore, settling and rising velocity investigations were carried out in addition to the concentration profile tests as these transfer the density and shape into a common factor. Table 3 shows the averaged values for all plastics used in the experiments. Furthermore, next to the shear stress velocity, the settling velocity is the most crucial factor of the Rouse number and the Rouse profile, respectively.

**Table 3. Settling Velocities of the Plastic Particles with Settling in the Positive Direction**

| polymer | settling velocity [m/s] | standard deviation |
|---|---|---|
| PA6 1 mm cubes | 0.0335 | 0.0013 |
| PA6 3 mm cylinders | 0.0591 | 0.0049 |
| PE-HD 3 mm granules | −0.0451 | 0.0054 |
| PP 1.5 mm spheres | −0.0396 | 0.0025 |

## 5. DISCUSSION

The individual influence of particle shape, particle density, particle weight, and particle surface volume ratio on the vertical transport behavior of the plastic particles in the experiments could not be clearly defined, first because of the small number of different particle types and second because of the simultaneous variation of several parameters between the particles. However, the settling or rising velocity binding all these particle properties into one parameter was found to be a well-working indicator. As shown in Table 3, the settling velocities do not differ proportionally to any particle property, such as diameter, as can be seen from the slight difference in the rising velocities of PP and PE-HD, despite double the diameter of PE-HD. This minor difference reflects in Figure 4 when comparing the concentration graphs of both buoyant plastic types.

Both PA6 particle types support the direct dependence of the concentration profiles on the settling velocity for the particle density range above 1 g/cm$^3$ (Figure 4). For example, with a nearly twice as high settling velocity of the 1 mm compared to the 3 mm PA6 particles, the latter's concentration in the graphs presented in Figure 4 is about 50% lower at the same depth and velocity. Furthermore, the graphs in Figure 5 demonstrate that the concentration−distribution−shift toward the water surface with increasing velocities for the PA6 particles can be well described by a quadratic interpolation. The exponential increase thus coincides with the calculation formula for the Rouse profile, likewise including an exponential approach.

No exponential relationship between the concentration shift and velocity could be obtained by analyzing the plastic particle types with a density below 1 g/cm$^3$, PE-HD, and PP (Figure 5). This divergence from both PA6 particle types' behavior might be attributable to insufficiently turbulent flow in the investigations and scarce data. Furthermore, the shift of the concentration profile toward the flume's bed is only clearly occurring at the highest flow velocity of 1.8 m/s (Figure 4), thus revealing that further tests at higher flow velocities beyond the flume's capacity are necessary for an improved understanding.

The key question of the investigations was whether Rouse's equations could be applied to plastic particles. The results in Figure 4 show that a Rouse-like profile is obtained for particles with a density above and running reversed for densities below the water density. However, whether Rouse's equation outputs a similar diagram and whether the formula also describes particles with a density below water's needs additional analyses.

In order to answer this question, the bed shear stress in the channel was determined (employing the water surface slope in eq 2), and the Rouse number was calculated employing the experimentally measured settling velocity (based on the assumption that $\tau_{turb} \approx \tau_0$ applies). Next, a Rouse profile was calculated and superimposed on the offset-adjusted measured profiles (Figure 7).

The graphs generally reveal a good fit of calculated and measured concentrations for all particle types used in the experiments. However, a deviation in the graphs becomes apparent, especially with increasing turbulences, most pronounced for 1 mm PA6 cubes at 1.5 m/s, most likely caused by the increased deviation from a uniform flow, which is a premise for eq 2. All further comparisons can be found in the Supporting Information (Figures S1−S4). Therefore, it can be concluded that the Rouse equation quite accurately describes the plastic concentration distribution for the plastic particles investigated. However, the deviation from the measured to calculated values intensifies with increasing velocities and turbulences. Thus, if a not uniform flow at high flow velocities is examined, the Rouse equation might not yield accurate results for the particle ranges considered in this study.

An extrapolation or transfer to other plastics cannot be concluded from this. However, it is reasonable to assume that for approximately spherical particles, like granules and pellets, the Rouse equation can be employed to calculate a distribution for MPs throughout the water column for the flume setup used in the experiments comparable to its accuracy for sediment. It is also reasonable to assume that the Rouse equation can be applied for MPs at near-uniform conditions in rivers. For validation of this assumption, however, further research is required.

Furthermore, the assumption was investigated whether the Rouse number range with reversed signs and a reference level close to the water surface is suitable for buoyant particles (Table 1). The graphs of calculated versus measured concentration in Figure 7 reveal a good fit for most of the experiments, thus supporting the experiment's central question.

However, while the ranges formulated by Rouse were observed for settling plastics, the classification by Cowger et al. (2021)[24] was not confirmed (Table 1; Supporting Information



https://doi.org/10.1021/acs.est.2c06885
Environ. Sci. Technol. 2023, 57, 5569−5579

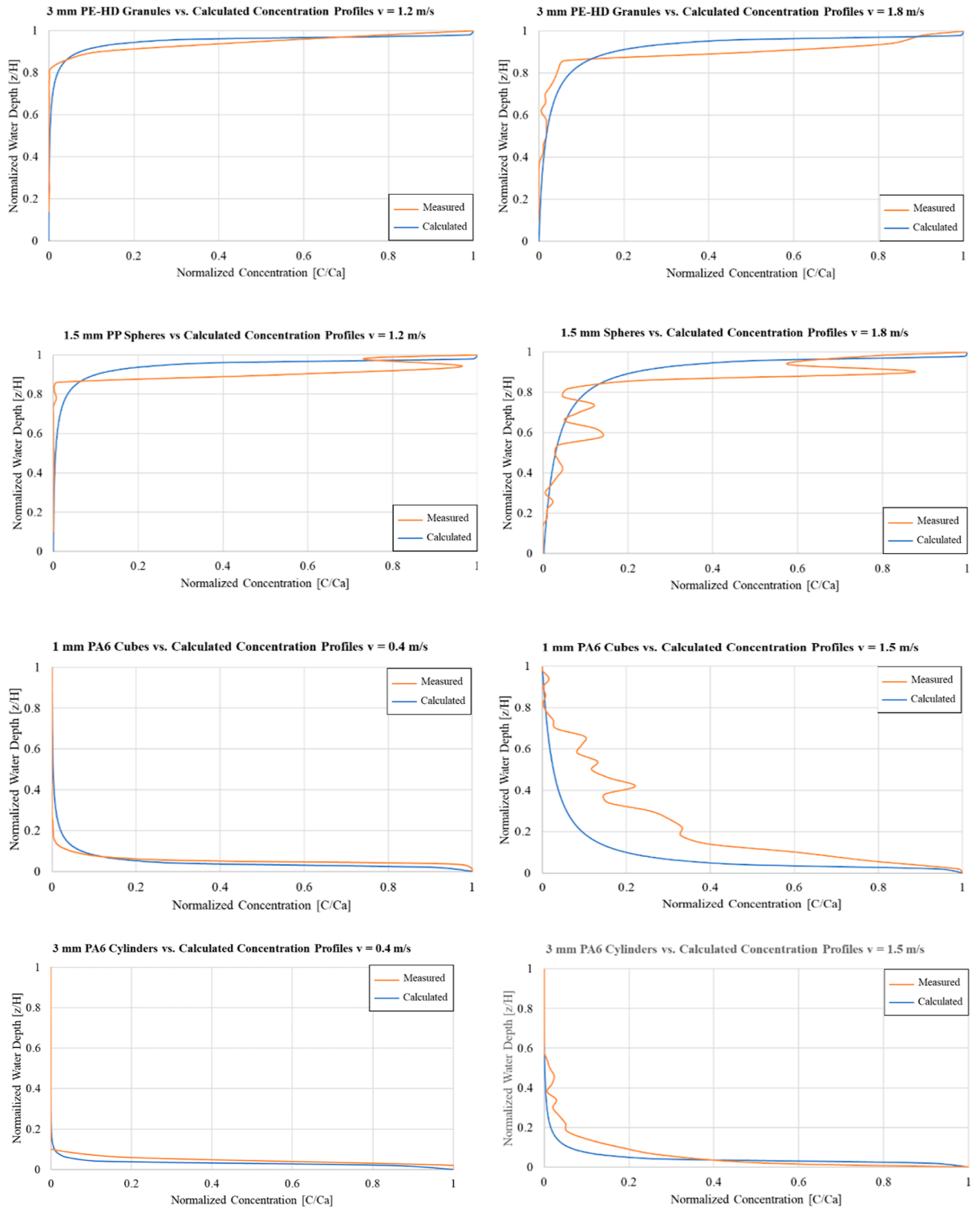


**Figure 7.** Comparison of calculated (blue) to measured (orange) concentration for the lowest and highest velocities.

Table S1). The results show, in part, that in many experimental runs, only surface transport was present, although, according to the classification, a strongly discernible suspended transport should have been visible. This is most likely attributable to the water surface tension and the general hydrophobicity of plastics, requiring an increased degree of turbulence to pull the particles underwater, delaying the onset of vertical particle transport.[45] However, particles can be vertically transported once the surface tension threshold is overcome and behave in accordance with the Rouse equation. This might explain the concordance of the measured results with the Rouse equation plot while the transport classification is proven incorrect.

Thus, a new classification was derived from the obtained values (Table 4). For the wash-load boundary, several extrapolations of flume settings were conducted. The values remain to be tested for different particles and hydraulic settings.



https://doi.org/10.1021/acs.est.2c06885
Environ. Sci. Technol. 2023, 57, 5569−5579

Table 4. Adjusted Rouse Number Transport Classification of MPs with a Density below 1 g/cm$^3$[a]

| range by Cowger et al. (2021)[24] | suggested Rouse number range | mode of transport |
|---|---|---|
| $-0.8 < P < 0.8$ | $-0.6 < P < 0.8$ | wash load |
| $-2.5 < P < -0.8$ | $-1.8 < P < -0.6$ | rising suspended transport |
| $P < -2.5$ | $P < -1.8$ | surface transport |

[a]Wash-load transport mode onset is defined at 50% particle concentration and at 50% water depth.

Generally, the results must be interpreted concerning the low water depths of 80 and 67 mm. Absolute small changes therethrough seemingly increase when plotted relatively, although maybe just a collision of two particles or minor local turbulence caused a slight descent or ascent.

## 6. GENERAL DISCUSSION

The experiments first investigate the vertical concentration profiles of MPs in flow channels. The measured profiles confirm the assumption that the concentration profile shapes of settling plastics are similar to those of natural sediments and running reversed for buoyant plastics. Furthermore, the Rouse formula's applicability hypothesis for buoyant and sinking plastics could be confirmed for approximately uniform flows. However, the degree of the result's applicability to plastic densities, sizes, and shapes beyond the tested particles cannot be approximated due to the experiment's scope. This would require a more extensive test series with numerous particle properties and hydraulic parameter variations. Especially with increasing turbulences and increasing deviations from a spherical shape and uniform flow, a divergent behavior of theory and practice is expected.

Future investigations should also vary the bed roughness in the test setup, either with a moving or fixed bed. This can cause increased local turbulences, which can influence the concentration distribution of the plastic particles under certain circumstances. A bed with increased roughness could also integrate effects such as hiding and exposure and thus represents field conditions more realistically. However, this could, in turn, adulterate particle tracking.

Another challenge for future experiments is increasing the effective shear stress, flow velocity, turbulence, and water depth, while the discharge remains filterable. For MP experiments, it is necessary to prevent particle re-entrainment, to not falsify the concentrations. A remedy could be finer particles of the same shape and density, which cannot be recorded by a camera but are evaluable via water samples. However, dispersal influences must be considered, and well-working separation, similar to an oil separator, included.

## ASSOCIATED CONTENT

### Supporting Information

The Supporting Information is available free of charge at https://pubs.acs.org/doi/10.1021/acs.est.2c06885.

Measured vs calculated concentration profiles for all plastic particles; Rouse profiles for all plastics; TKE distribution for all velocities and water depths; Rouse numbers for all plastic types; and information on experimental settings (PDF)

## AUTHOR INFORMATION


### Corresponding Author

**Maximilian P. Born** − *Institute of Hydraulic Engineering and Water Resources Management, RWTH-Aachen University, 52074 Aachen, Germany;* orcid.org/0000-0002-1766-0131; Phone: +49 (0) 241 80 25269; Email: born@iww.rwth-aachen.de

### Authors

**Catrina Brüll** − *Institute of Hydraulic Engineering and Water Resources Management, RWTH-Aachen University, 52074 Aachen, Germany*

**Dirk Schaefer** − *Federal Institute for Hydrology, 56068 Koblenz, Germany*

**Gudrun Hillebrand** − *Federal Institute for Hydrology, 56068 Koblenz, Germany;* orcid.org/0000-0003-1489-9443

**Holger Schüttrumpf** − *Institute of Hydraulic Engineering and Water Resources Management, RWTH-Aachen University, 52074 Aachen, Germany;* orcid.org/0000-0002-0104-0499

Complete contact information is available at: https://pubs.acs.org/10.1021/acs.est.2c06885


### Notes

The authors declare no competing financial interest.

## ACKNOWLEDGMENTS

The authors would like to thank all their colleagues assisting during the experiments, especially the student assistances Janine Freyer and Benedikt Bröcker. The German Federal Institute for Hydrology funded this research. Furthermore, the authors would like to thank the *Institute for Textile Technology of RWTH Aachen University* for supplying a variety of plastics. In addition, the authors would like to thank the *PIA GmbH* for lending the vibrating feeder.

## REFERENCES


(1) Freyer, J. Analyse der vertikalen Konzentrationsverteilung von Mikroplastikpartikeln in Fließrinnen (not published). Master Thesis, RWTH Aachen University, 2023. Supervision by: Maximilian P. Born.

(2) Geyer, R.; Jambeck, J. R.; Law, K. L. Production, use, and fate of all plastics ever made. *Sci. Adv.* **2017**, *3*, No. e1700782.

(3) Lechthaler, S.; Waldschläger, K.; Stauch, G.; Schüttrumpf, H. The Way of Macroplastic through the Environment. *Environments* **2020**, *7*, 73.

(4) Waldschläger, K.; Lechthaler, S.; Stauch, G.; Schüttrumpf, H. The way of microplastic through the environment - Application of the source-pathway-receptor model (review). *Sci. Total Environ.* **2020**, *713*, 136584.

(5) Andrady, A. L. Microplastics in the marine environment. *Mar. Pollut. Bull.* **2011**, *62*, 1596−1605.

(6) Born, M. P.; Brüll, C. From model to nature - A review on the transferability of marine (micro-) plastic fragmentation studies. *Sci. Total Environ.* **2022**, *811*, 151389.

(7) Hartmann, N. B.; Hüffer, T.; Thompson, R. C.; Hassellöv, M.; Verschoor, A.; Daugaard, A. E.; Rist, S.; Karlsson, T.; Brennholt, N.; Cole, M.; Herrling, M. P.; Hess, M. C.; Ivleva, N. P.; Lusher, A. L.; Wagner, M. Are We Speaking the Same Language? Recommendations for a Definition and Categorization Framework for Plastic Debris. *Environ. Sci. Technol.* **2019**, *53*, 1039−1047.

(8) Frias, J. P. G. L.; Nash, R. Microplastics: Finding a consensus on the definition. *Mar. Pollut. Bull.* **2019**, *138*, 145−147.

(9) Gasperi, J.; Dris, R.; Bonin, T.; Rocher, V.; Tassin, B. Assessment of floating plastic debris in surface water along the Seine River. *Environ. Pollut.* **2014**, *195*, 163−166.

(10) Jambeck, J. R.; Geyer, R.; Wilcox, C.; Siegler, T. R.; Perryman, M.; Andrady, A.; Narayan, R.; Law, K. L. Plastic waste inputs from land into the ocean. *Science* **2015**, *347*, 768−771.
(11) Ballerini, T.; Le Pen, J.-R.; Andrady, A.; Cole, M.; Galgani, F.; Kedzierski, M.; Pedrotti, M. L.; Ter Halle, A.; Van Arkel, K.; Zettler, E.; Amaral-Zettler, L.; Bruzaud, S.; Brandon, J.; Durand, G.; Enevoldsen, E.; Eriksen, M.; Fabre, P.; Fossi, M.-C.; Frère, L.; Avio, C. G.; Hardesty, D.; Jambeck, J.; Lavender, K.; Mansui, J.; Nafrechoux, E.; Schmidt, C.; Sempéré, R.; Thiel, M.; Thomson, R.; Wong-Wha-Chung, P. *Plastic Pollution in the Ocean: What We Know and what We Don't Know about*; Plastic and Ocean Platform, 2018.
(12) Rochman, C. M. Microplastics research-from sink to source. *Science* **2018**, *360*, 28−29.
(13) Liubartseva, S.; Coppini, G.; Lecci, R.; Creti, S. Regional approach to modeling the transport of floating plastic debris in the Adriatic Sea. *Mar. Pollut. Bull.* **2016**, *103*, 115−127.
(14) Chassignet, E. P.; Xu, X.; Zavala-Romero, O. Tracking Marine Litter With a Global Ocean Model: Where Does It Go? Where Does It Come From? *Front. Mar. Sci.* **2021**, *8*, 667591.
(15) Zhang, Z.; Wu, H.; Peng, G.; Xu, P.; Li, D. Coastal ocean dynamics reduce the export of microplastics to the open ocean. *Sci. Total Environ.* **2020**, *713*, 136634.
(16) Chenillat, F.; Huck, T.; Maes, C.; Grima, N.; Blanke, B. Fate of floating plastic debris released along the coasts in a global ocean model. *Mar. Pollut. Bull.* **2021**, *165*, 112116.
(17) Waldschläger, K. L.; Hollert, H.; Schüttrumpf, H. Transport Processes of Microplastic Particles in the Fluvial Environment: Erosion, Transport and Deposition. PhD Thesis, RWTH Aachen University, 2020.
(18) Jalón-Rojas, I.; Romero-Ramírez, A.; Fauquembergue, K.; Rossignol, L.; Cachot, J.; Sous, D.; Morin, B. Effects of Biofilms and Particle Physical Properties on the Rising and Settling Velocities of Microplastic Fibers and Sheets. *Environ. Sci. Technol.* **2022**, *56*, 8114−8123.
(19) Kooi, M.; Nes, E. H.; Scheffer, M.; Koelmans, A. A. Ups and Downs in the Ocean: Effects of Biofouling on Vertical Transport of Microplastics. *Environ. Sci. Technol.* **2017**, *51*, 7963−7971.
(20) Xia, F.; Yao, Q.; Zhang, J.; Wang, D. Effects of seasonal variation and resuspension on microplastics in river sediments. *Environ. Pollut.* **2021**, *286*, 117403.
(21) Xia, W.; Rao, Q.; Deng, X.; Chen, J.; Xie, P. Rainfall is a significant environmental factor of microplastic pollution in inland waters. *Sci. Total Environ.* **2020**, *732*, 139065.
(22) Rouse, H. Modern Conceptions of the Mechanics of Fluid Turbulence. *Trans. Am. Soc. Civ. Eng.* **1937**, *102*, 463−505.
(23) Cheng, C.; Song, Z.; Wang, Y.; Zhang, J. Parameterized expressions for an improved Rouse equation. *Int. J. Sediment Res.* **2013**, *28*, 523−534.
(24) Cowger, W.; Gray, A. B.; Guilinger, J. J.; Fong, B.; Waldschläger, K. Concentration Depth Profiles of Microplastic Particles in River Flow and Implications for Surface Sampling. *Environ. Sci. Technol.* **2021**, *55*, 6032−6041.
(25) Muste, M.; Yu, K.; Fujita, I.; Ettema, R. Two-phase flow insights into open-channel flows with suspended particles of different densities. *Environ. Fluid Mech.* **2009**, *9*, 161−186.
(26) Ballent, A.; Purser, A.; de Jesus Mendes, P.; Pando, S.; Thomsen, L. Physical transport properties of marine microplastic pollution. *Biogeosci. Discuss.* **2012**, *9*, 18755−18798.
(27) Shamskhany, A.; Li, Z.; Patel, P.; Karimpour, S. Evidence of Microplastic Size Impact on Mobility and Transport in the Marine Environment: A Review and Synthesis of Recent Research. *Front. Mar. Sci.* **2021**, *8*, 760649.
(28) Waldschläger, K.; Schüttrumpf, H. Effects of Particle Properties on the Settling and Rise Velocities of Microplastics in Freshwater under Laboratory Conditions. *Environ. Sci. Technol.* **2019**, *53*, 1958−1966.
(29) Waldschläger, K.; Born, M.; Cowger, W.; Gray, A.; Schüttrumpf, H. Settling and Rising Velocities of Environmentally Weathered Micro- and Macroplastic Particles. *Environ. Res.* **2020**, *191*, 110192.
(30) Kuizenga, B.; van Emmerik, T.; Waldschläger, K.; Kooi, M. Will it float? Rising and settling velocities of common macroplastic foils. *ACS ES&T Water* **2022**, *2*, 975.
(31) Vercruysse, K.; Grabowski, R. C.; Rickson, R. J. Suspended sediment transport dynamics in rivers: Multi-scale drivers of temporal variation. *Earth-Sci. Rev.* **2017**, *166*, 38−52.
(32) Rijn, L. C. Sediment Transport, Part II: Suspended Load Transport. *J. Hydraul. Eng.* **1984**, *110*, 1613−1641.
(33) Bennett, S. J.; Bridge, J. S.; Best, J. L. Fluid and sediment dynamics of upper stage plane beds. *J. Geophys. Res.* **1998**, *103*, 1239−1274.
(34) Nikora, V. I.; Goring, D. G. Fluctuations of Suspended Sediment Concentration and Turbulent Sediment Fluxes in an Open-Channel Flow. *J. Hydraul. Eng.* **2002**, *128*, 214−224.
(35) Kumbhakar, M.; Ghoshal, K.; Singh, V. P. Derivation of Rouse equation for sediment concentration using Shannon entropy. *Phys. A* **2017**, *465*, 494−499.
(36) Manica, R. *Hydrodynamics—Natural Water Bodies*; Schulz, H. E., Ed.; InTech, 2012.
(37) Pope, S. B. *Turbulent Flows*; Cambridge University Press, 2012.
(38) Van Melkebeke, M.; Janssen, C.; De Meester, S. Characteristics and Sinking Behavior of Typical Microplastics Including the Potential Effect of Biofouling: Implications for Remediation. *Environ. Sci. Technol.* **2020**, *54*, 8668−8680.
(39) Karkanorachaki, K.; Syranidou, E.; Kalogerakis, N. Sinking characteristics of microplastics in the marine environment. *Sci. Total Environ.* **2021**, *793*, 148526.
(40) Meltytech, L. *Shotcut*; Meltytech, LLC, 2022.
(41) Schindelin, J.; Arganda-Carreras, I.; Frise, E.; Kaynig, V.; Longair, M.; Pietzsch, T.; Preibisch, S.; Rueden, C.; Saalfeld, S.; Schmid, B.; Tinevez, J.-Y.; White, D. J.; Hartenstein, V.; Eliceiri, K.; Tomancak, P.; Cardona, A. Fiji: an open-source platform for biological-image analysis. *Nat. Methods* **2012**, *9*, 676−682.
(42) Ershov, D.; Phan, M.-S.; Pylvänäinen, J. W.; Rigaud, S. U.; Le Blanc, L.; Charles-Orszag, A.; Conway, J. R. W.; Laine, R. F.; Roy, N. H.; Bonazzi, D.; Duménil, G.; Jacquemet, G.; Tinevez, J.-Y. Bringing TrackMate into the era of machine-learning and deep-learning. **2021**, bioRxiv 2021.09.03.458852.
(43) Tinevez, J.-Y.; Perry, N.; Schindelin, J.; Hoopes, G. M.; Reynolds, G. D.; Laplantine, E.; Bednarek, S. Y.; Shorte, S. L.; Eliceiri, K. W. TrackMate: An open and extensible platform for single-particle tracking. *Methods* **2017**, *115*, 80−90.
(44) *MATLAB*; The MathWorks Inc.: Natick, Massachusetts; 2023.
(45) Valero, D.; Belay, B. S.; Moreno-Rodenas, A.; Kramer, M.; Franca, M. J. The key role of surface tension in the transport and quantification of plastic pollution in rivers. *Water Res.* **2022**, *226*, 119078.


https://doi.org/10.1021/acs.est.2c06885
Environ. Sci. Technol. 2023, 57, 5569−5579